of Basic Energy Sciences, for support of this work. M.T., A.K., and S.R.L. acknowledge the Department of Education for research fellowships, and C.N. acknowledges the National Science Foundation for a predoctoral fellowship. We also thank Professor Edward M. Stolper for providing the Spectra Span VB Emission Spectrometer (DCP Emission Spectrometer) and Sally Newman for assistance with the operation of the spectrometer.

Registry No. GaAs, 1303-00-0; K_2Se, 1312-74-9; K_2Se_2, 12794-75-1; K_2Te, 12142-40-4; K_2Te_2, 78547-42-9; KOH, 1310-58-3; In_2O_3, 1312-43-2; Sn, 7440-31-5; $[Co(NH_3)_6]Cl_3$, 10534-89-1; $OsCl_3$, 13444-93-4; $RuCl_3$, 10049-08-8; K_2OsCl_6, 16871-60-6; Br_2, 7726-95-6; MeOH, 67-56-1.

Photochemical Hole-Burning Spectroscopy of a Photosynthetic Reaction Center Mutant with Altered Charge Separation Kinetics: Properties and Decay of the Initially Excited State

Thomas R. Middendorf,[†] Laura T. Mazzola,[†] Dale F. Gaul,[‡] Craig C. Schenck,[‡] and Steven G. Boxer*,[†]

Department of Chemistry, Stanford University, Stanford, California 94305, and Department of Biochemistry, Colorado State University, Fort Collins, Colorado 80523 *(Received: April 15, 1991; In Final Form: July 15, 1991)*

Photochemical hole-burning spectra have been obtained for the lowest energy electronic absorption band of the primary electron donor P of photosynthetic reaction centers (RCs) that exhibit different rates for the initial charge separation step. Wild type (WT) and Tyr(M)210 → Phe mutant [(M)Y210F] RCs from *Rhodobacter sphaeroides* were studied at 1.5 K in 50% glycerol/buffer glasses. In both types of RC, difference spectra obtained by using narrow-bandwidth excitation on the low-energy edge of the P band display weak, narrow zero-phonon holes coincident with the laser wavelengths, in addition to a broad background bleach of much larger amplitude. The zero-phonon hole width in each type of RC corresponds quantitatively to the broadening expected from the excited-state lifetime. These results are inconsistent with electronic relaxation of the excited state of P prior to electron transfer. The agreement between the time- and frequency-domain experiments may result from vibrational thermalization prior to electron transfer. An alternative mechanism, which does not invoke subpicosecond vibrational thermalization and which is consistent with a wide range of data, is also presented. Quantitative estimates were obtained for the total electron–phonon coupling strength (Huang–Rhys factor) S and for the magnitudes of the homogeneous and inhomogeneous broadening in the P absorption band from self-consistent simulations of the 1.5 K absorption and hole spectra from a linear electron–phonon coupling model. The vibronic and line-width parameters deduced from the simulations are very similar for WT and (M)Y210F RCs.

The mechanism of the initial charge separation step in bacterial photosynthetic reaction centers (RCs) is a subject of continuing controversy. As with any reaction mechanism, it is essential to establish the nature of the initial, intermediate, and final states and the kinetics that connect these states. In spite of detailed structural[1-3] and kinetic[4-8] information, it has proven remarkably difficult to reach a unified description of the relevant states. Recently, several groups have used photochemical hole burning[9-17] and RCs modified by site-directed mutagenesis[18-23] to supplement the structural[1-3] and kinetic[4-8] information that provide the traditional basis for mechanistic studies. These methods are combined in the present study.

A schematic illustration of the reactive components in the RC is shown in Figure 1. It is generally agreed that the state which initiates charge separation is the lowest singlet excited state of the special pair, ^1P, though the origin and the degree of charge asymmetry in this state is still an open and important question. The final state is the charge-separated state $P^+H_L^-$, where the symbol H_L is used to denote a bacteriopheophytin electron acceptor. It is generally agreed that within 3.5 ps an electron has moved to H_L in wild-type RCs at room temperature. There is a continuing debate concerning the role of the bacteriochlorophyll *a* molecule labeled B_L. Some kinetic evidence suggests that the anion of this molecule is a discrete intermediate ($P^+B_L^-$) between ^1P and $P^+H_L^-$;[24] other kinetic[5-8] and electric field effect[25-27] data indicate that $P^+B_L^-$ is not an intermediate. If the latter is the case, it is likely that states such as $P^+B_L^-$[28,29] or ^1B_L[29] serve to mediate the coupling between ^1P and $P^+H_L^-$.[30]

Whether the initial electron transfer reaction occurs via a two-step hopping or superexchange mechanism involving $P^+B_L^-$,

[†] Stanford University.
[‡] Colorado State University.

(1) Michel, H.; Epp, O.; Diesenhofer, J. *EMBO J.* **1986**, *5*, 2445.
(2) Allen, J. P.; Feher, G.; Yeates, T. O.; Komiya, H.; Rees, D. C. *Proc. Natl. Acad. Sci. U.S.A.* **1987**, *84*, 5730.
(3) Chang, C. H.; Tiede, D.; Tang, J.; Smith, U.; Norris, J. *FEBS Lett.* **1986**, *205*, 82.
(4) Woodbury, N. W.; Becker, M.; Middendorf, D.; Parson, W. W. *Biochemistry* **1985**, *24*, 7516.
(5) Kirmaier, C.; Holten, D. *FEBS Lett.* **1988**, *239*, 211.
(6) Breton, J.; Martin, J.-L.; Fleming, G. R.; Lambry, J. C. *Biochemistry* **1988**, *27*, 8276.
(7) Kirmaier, C.; Holten, D. *Biochemistry* **1991**, *30*, 609.
(8) Fleming, G. R.; Martin, J.-L.; Breton, J. *Nature* **1988**, *333*, 190.
(9) Boxer, S. G.; Lockhart, D. J.; Middendorf, T. R. *Chem. Phys. Lett.* **1986**, *123*, 476.
(10) Boxer, S. G.; Middendorf, T. R.; Lockhart, D. J. *FEBS Lett.* **1986**, *200*, 237.
(11) Meech, S. R.; Hoff, A. J.; Wiersma, D. A. *Chem. Phys. Lett.* **1985**, *121*, 287.
(12) Meech, S. R.; Hoff, A. J.; Wiersma, D. A. *Proc. Natl. Acad. Sci. U.S.A.* **1986**, *83*, 9464.
(13) Ganago, A. O.; Melkozernov, A. N.; Shuvalov, V. A. *Biophysics* **1986**, *31*, 481.
(14) Tang, D.; Jankowiak, R.; Gillie, J. K.; Small, G. J.; Tiede, D. M. *J. Phys. Chem.* **1988**, *92*, 4012.
(15) Johnson, S. G.; Tang, D.; Jankowiak, R.; Hayes, J. M.; Small, G. J.; Tiede, D. M. *J. Phys. Chem.* **1989**, *93*, 5953.
(16) Tang, D.; Johnson, S. G.; Jankowiak, R.; Hayes, J. M.; Small, G. J.; Tiede, D. M. In *Twenty Second Jerusalem Symposium: Perspectives in Photosynthesis*; Jortner, J., Pullman, B., Eds.; Kluwer Academic: Dordrecht, 1990; p 99.
(17) Johnson, S. G.; Tang, D.; Jankowiak, R.; Hayes, J. M.; Small, G. J.; Tiede, D. M. *J. Phys. Chem.* **1990**, *94*, 5849.
(18) Nagarajan, V.; Parson, W. W.; Gaul, D.; Schenck, C. *Proc. Natl. Acad. Sci. U.S.A.* **1990**, *87*, 7888.

0022-3654/91/2095-10142$02.50/0

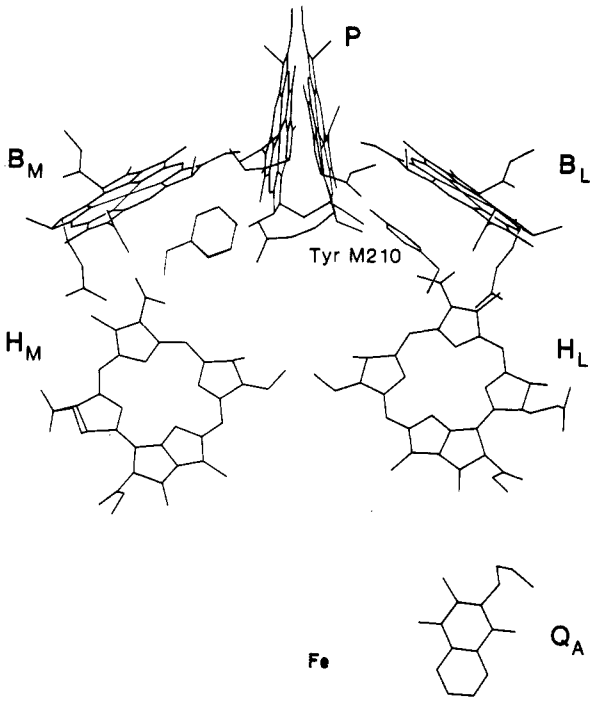

Figure 1. Schematic diagram of the arrangement of the chromophores in the bacterial reaction center based on the X-ray structure.[1-3] The location of Tyr(M)210 is also indicated.

the rate of the reaction should depend on the energy of the $P^+B_L^-$ state. To date there is no direct information on this energy; however, a first step has been taken by Warshel and Parson to estimate the free energy of this state by using free-energy perturbation molecular dynamics simulations.[31] These simulations suggest that Tyr(M)210, which is adjacent to B_L and is in van der Waals contact with all of the L-side chromophores (see Figure 1), may significantly stabilize the hypothetical B_L anion. Furthermore, this stabilization is not available for the hypothetical B_M anion on the nonfunctioning M branch of the RC, which has a phenylalanine in the position equivalent to Tyr(M)210. A more specific and difficult question is whether the absolute free energy estimated for the hypothetical $P^+B_L^-$ state is below ^1P, as this is a necessary, though not sufficient, condition if $P^+B_L^-$ is to be a populated intermediate state at low temperature. The accuracy of the calculations is not at present adequate to determine the relative energies of these states.

In order to further understand the role of Tyr(M)210, this residue has been changed to phenylalanine [(M)Y210F] and to several other nonpolar residues by site-directed mutagenesis.[18,32-34] For *Rhodobacter sphaeroides*, a significant slowing of the $^1P \rightarrow P^+H_L^-$ kinetics was measured for (M)Y210F, $(10.5\ ps)^{-1}$, compared to the wild-type, $(3.5\ ps)^{-1}$ at room temperature and $(10\ ps)^{-1}$ versus $(1.9\ ps)^{-1}$ at 80 K.[18] This effect indicates that Tyr(M)210 plays a significant role in the initial electron transfer step but does not identify whether the Tyr → Phe substitution primarily affects the reactants, the products, or the coupling between them.

Photochemical hole burning offers an alternative to time-resolved spectroscopy, which takes advantage of several features of the RC. First, the lowest electronic absorption band of P is largely bleached upon formation of P^+. Second, the initial photochemistry and secondary charge separation and recombination reactions have rates that are nearly independent of temperature. Thus at the cryogenic temperatures required for hole-burning experiments, the quantum yield for P^+ formation remains high and the bleach of the special pair ground-state absorption persists for many milliseconds. Third, hole-burning spectroscopy may yield information on the magnitude of vibronic coupling[35] in the P absorption band as well as vibrational structure in the transition, which is masked by inhomogeneous broadening.

The original photochemical hole-burning experiments on *Rb. sphaeroides*, R-26.1 (carotenoidless) mutant, and *Rhodopseudomonas viridis* (RCs) demonstrated that essentially the entire band is bleached following narrow-bandwidth excitation of P at several wavelengths within its lowest energy electronic absorption band.[9-12] These results contrast with the simple expectation of a rather narrow (about 10 cm^{-1}) hole if the hole width were determined entirely by the excited-state lifetime of ^1P, which has been measured in transient absorption experiments.[4,6,36] Two interpretations that are consistent with these observations were presented.[9-12] The first of these suggested that the observed hole is a zero-phonon hole that is extremely broad due to rapid electronic relaxation (~20–200 fs) of the initial excited state.[9-12] Alternatively, Boxer et al.[9,10] suggested that if ^1P contains a substantial amount of charge transfer character, then "the formation of such a state from the neutral ground state would involve a large difference in the equilibrium nuclear configuration between the ground and excited state. Such a difference could lead to the suppression of the zero-phonon line".[10] In the latter model, the absence of structure in the hole results from a manifold of unresolvable vibronic and/or phonon transitions within the P band. Quantitative theoretical treatments related to this second proposal were presented later that detailed the effects of strong electron–phonon coupling in the P band[37,38] and exchange coupling between ^1P and another nearly resonant electronic state.[39]

(19) Bylina, E. J.; Youvan, D. *Proc. Natl. Acad. Sci. U.S.A.* **1988**, *85*, 7226.
(20) Hammes, S. L.; Mazzola, L. T.; Boxer, S. G.; Gaul, D. F.; Schenck, C. C. *Proc. Natl. Acad. Sci. U.S.A.* **1990**, *87*, 5682.
(21) Kirmaier, C.; Holten, D.; Bylina, E. J.; Youvan, D. C. *Proc. Natl. Acad. Sci. U.S.A.* **1988**, *85*, 7562.
(22) Mattioli, T. A.; Gray, K. A.; Lutz, M.; Oesterhelt, D.; Robert, B. *Biochemistry* **1991**, *30*, 1715.
(23) Kirmaier, C.; Gaul, D.; DeBey, R.; Holten, D.; Schenck, C. C. *Science* **1991**, *251*, 922.
(24) Holzapfel, W.; Finkele, U.; Kaiser, W.; Oesterhelt, D.; Scheer, H.; Stilz, H. U.; Zinth, W. *Chem. Phys. Lett.* **1989**, *160*, 1.
(25) Lockhart, D. J.; Goldstein, R. F.; Boxer, S. G. *J. Chem. Phys.* **1988**, *88*, 1408.
(26) Lockhart, D. J.; Kirmaier, C.; Holten, D.; Boxer, S. G. *J. Phys. Chem.* **1990**, *94*, 6987.
(27) Bixon, M.; Jortner, J.; Michel-Beyerle, M.-E. In *Reaction Centers of Photosynthetic Bacteria*; Michel-Beyerle, M.-E., Ed.; Springer-Verlag: Berlin, 1990; p 389.
(28) Michel-Beyerle, M. E.; Plato, M.; Deisenhofer, J.; Michel, H.; Bixon, M.; Jortner, J. *Biochim. Biophys. Acta* **1988**, *932*, 52.
(29) Boxer, S. G.; Goldstein, R. A.; Lockhart, D. J.; Middendorf, T. R.; Takiff, L. *J. Phys. Chem.* **1989**, *93*, 8280.
(30) We note at the outset that although it is common to describe intermediates as ion pair states, there is, in fact, little information on the charge distribution of the intermediates on the picosecond time scale. While it is certainly reasonable to consider these short-lived intermediates to be charged, it is possible that, on some time scale, protons or other groups may move, compensating to some degree for the charges. Free energy perturbation calculations such as those in ref 31 likewise begin with the assertion that the charge is on a specific molecule.
(31) Parson, W. W.; Chu, Z. T.; Warshel, A. *Biochim. Biophys. Acta* **1990**, *1017*, 251.
(32) Gaul, D.; Brasher, B.; Martin, K.; Schenck, C. *Biophys. J.* **1989**, *55*, 181a.
(33) Gray, K. A.; Farchaus, J. W.; Wachtveitl, J.; Breton, J.; Oesterhelt, D. *EMBO J.* **1990**, *9*, 2061.
(34) Chan, C.-K.; Chen, L.; DiMagno, T. J.; Hanson, D. K.; Nance, S. L.; Schiffer, M.; Norris, J. R.; Fleming, G. R. *Chem. Phys. Lett.* **1991**, *176*, 366.
(35) Because of the uncertain identification of the modes that are coupled to the $P \rightarrow {}^1P$ transition, the terms vibronic coupling and electron–phonon coupling will be used interchangeably in this paper.
(36) Kirmaier, C.; Holten, D. *Photosynth. Res.* **1987**, *13*, 225.
(37) Hayes, J. M.; Small, G. J. *J. Phys. Chem.* **1986**, *90*, 4928.
(38) Hayes, J. M.; Gillie, J. K.; Tang, D.; Small, G. J. *Biochim. Biophys. Acta* **1988**, *932*, 287.
(39) Won, Y.; Friesner, R. A. *J. Phys. Chem.* **1988**, *92*, 2214. This model ascribes the relatively structureless hole-burning spectra of P to vibronic coupling between the excited state of P and another, nearly resonant electronic state. We have opted to use the Huang–Rhys model with a single electronic transition for the purpose of computational simplicity, while noting that models involving additional electronic states may be equally consistent with the available data. There is no definitive evidence at this time for the existence or identity of such a state. We stress that conclusions concerning the magnitude of S_{total} and the dynamics of ^1P from our analysis are dependent on the assumption that the P band is composed of a single electronic transition.

Subsequent experiments indicated that a very weak, narrow, zero-phonon hole is present at the burn wavelength in *Rb. sphaeroides* and *Rps. viridis* RCs but only when the excitation was tuned to the low-energy tail of the special pair absorption band.[13-17] In both species the width of this feature corresponded, within the experimental error, to the excited-state lifetime of ^1P measured in transient absorption experiments at 10 K. However, the lifetime of ^1P at this temperature in the two types of RCs is very similar, and, due to the very small amplitude of the zero-phonon feature, the relative uncertainties in the zero-phonon hole widths are substantial. A series of different interpretations were offered to explain the much more intense broad sideband hole and possible substructure,[14,15,38,40] culminating in experimental data and an analysis[16,17] that are similar to those discussed below for wild-type RCs, with some modifications. The possible correlation between the excited-state lifetime and the zero-phonon hole width is an important result, and we were prompted to further test it by measuring the hole-burning spectrum of an RC with significantly altered charge separation kinetics. The lifetime of ^1P has been measured at 80 K in the (M)Y210F mutant of *Rb. sphaeroides* and is six times longer than in wild-type (WT) RCs at that temperature.[18] Given the similarity in the magnitude and temperature dependence of this rate between wild-type and R-26 RCs (where the lifetime has been measured down to 10 K) and the temperature independence of the rate in (M)Y210F,[18] the lifetime is expected to be eight times longer in (M)Y210F than in WT at liquid He temperatures. If the assertion that the zero-phonon hole width is determined by the electronic lifetime of ^1P is correct, then the hole width should then be a factor of 8 narrower in the mutant; this is in fact observed (vide infra). A preliminary account of this work has been presented elsewhere.[41]

Materials and Methods

Wild-type and (M)Y210F *Rb. sphaeroides* RCs were prepared as previously described.[4] RCs in 0.01% LDAO, 10 mM Tris, pH 8, 20 mM NaCl were diluted with glycerol to yield a final solvent composition of 50% (v/v) glycerol/buffer. RC concentrations were typically 1×10^{-4} M.

RCs in 50% glycerol/buffer were placed in sample cells consisting of two glass slides separated by a 500-μm spacer and were rapidly frozen by immersion into liquid N_2 in a liquid helium dewar. The liquid N_2 was then removed by suction, and the dewar was filled with liquid He. Temperatures of $\sim$1.5 K were achieved by lowering the vapor pressure of the liquid He by mechanical pumping. The sample temperature was monitored by using a Si diode temperature sensor (DT471-SD, Lake Shore Cryotronics) and by measurement of the vapor pressure above the liquid He using a calibrated manometer (Validyne Corp.).

A temperature-stabilized CW strained-layer InGaAs quantum well diode laser (Polaroid Corp.) was used as the excitation source in the experiments. The output of these multimode lasers consists of a series of lines with typical line widths of 0.5-cm^{-1} fwhm and an average spacing of 3.0 cm^{-1} (see Figure 4). To ensure spatial spectral homogeneity of the laser output, microscope objectives were used to collect and focus the laser emission into a 10-m long, 50-μm diameter fiber optic cable; the beam emerging from the output end of the fiber was then focused onto the sample. The typical burn power was 6 mW/cm^2 at the sample. The laser diode spectrum was measured before and after the high-resolution hole-burning spectra. The absolute frequency drift of the laser lines was typically <0.1 cm^{-1} and over the course of an experiment (typically several hours) the relative intensity variations of the individual output lines were typically 15% or less.

Light from a tungsten–halogen bulb dispersed with a $^3/_4$-m monochromator and detected with a Si avalanche photodiode (C30956E, RCA) was used to probe the transmission of the sample. The transmission spectrum of the sample after irradiation was obtained by alternately opening and closing mechanical shutters operating at 10 Hz in front of the laser diode and probe light detector and measuring the resulting signal with lock-in detection. Typically, the transmission was probed for a period of $\sim$20 ms, starting 3 ms after the burn light was blocked. The difference absorption (hole) spectrum of the sample was obtained from the transmission spectra of the sample taken in the presence and absence of burn light. Control experiments on glycerol/buffer blanks were performed to ensure that there were no artifacts in the hole-burning spectra due to scattered laser light. The maximum change in absorption in the broad component of the holes was always kept to 20% or less of the total absorption. The magnitude of the holes scaled linearly with laser intensity for the burn powers employed. For the high-resolution hole-burning scans, the monochromator bandwidth was 0.65 cm^{-1}. Absorption spectra were obtained from the transmission spectra of the sample and an appropriate glycerol/buffer blank.

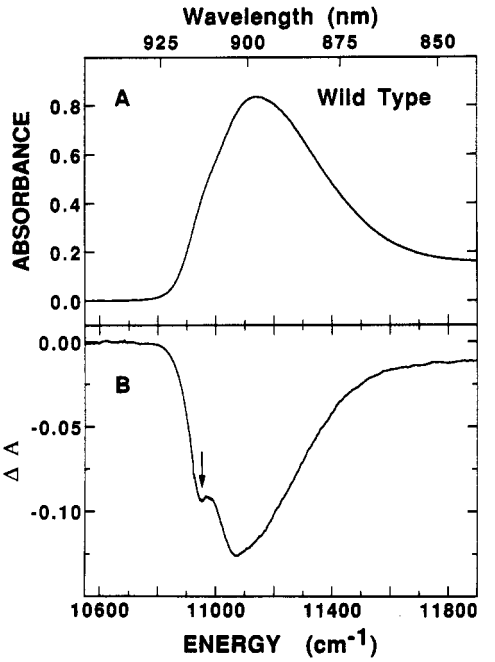

Figure 2. Absorption (A) and photochemical hole-burning spectra (B) for the lowest electronic transition of *Rb. sphaeroides* wild-type RCs in 50% (v/v) glycerol/buffer at 1.5 K. The center of the group of lines from the laser diode used to burn the hole (see Figure 4) is indicated by the arrow. Spectrum B was obtained by splicing the hole spectrum in the region of the burn laser taken at high resolution (0.65 cm^{-1}) into the hole spectrum taken under lower resolution (5 cm^{-1}) conditions, ensuring that the relative amplitudes of the narrow and broad features are accurately represented.

Results

The absorption and change in absorption following the burn for WT and (M)Y210F RCs are shown in Figures 2 and 3, respectively, for the lowest energy electronic transition of P at 1.5 K. As seen in all previous experiments,[9-17] the hole-burning spectrum is dominated by a very broad hole. The widths of the broad components of the holes are 404- and 397-cm^{-1} fwhm in WT and (M)Y210F, respectively; the corresponding absorption widths are 485- and 450-cm^{-1} fwhm. Thus a large fraction of the broadening in the P band of these RCs is homogeneous in nature. We find no evidence for further substructure within the broad holes for these strains.

In addition to the broad component of the hole, a very weak narrow feature is observed at the burn wavelength in WT and (M)Y210F RCs. The hole spectra of WT and (M)Y210F RCs in the vicinity of the burn frequencies are shown at high resolution in Figure 4, along with the spectrum of the laser diode output used to burn the holes. The hole spectra for both types of RC were obtained under identical conditions. The correlation between the excited-state lifetimes and the zero-phonon hole widths in these RCs is immediately apparent. The multiple lines in the diode

(40) Tang, D.; Jankowiak, R.; Small, G. J. *Chem. Phys.* **1989**, *131*, 99.
(41) Middendorf, T. R.; Mazzola, L. T.; Boxer, S. G.; Gaul, D.; Schenck, C. C. *Biophys. J.* **1991**, *59*, 141a (abstract).

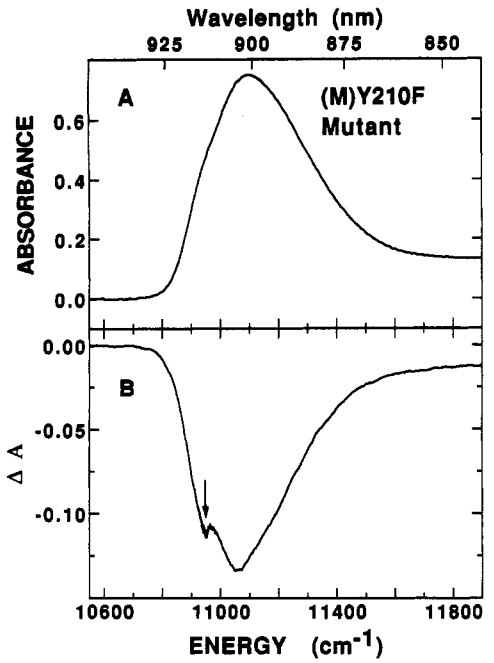

Figure 3. Absorption (A) and photochemical hole-burning spectra (B) for the lowest electronic transition of *Rb. sphaeroides* (M)Y210F mutant RCs in 50% (v/v) glycerol/buffer at 1.5 K. The center of the group of lines from the laser diode used to burn the hole (see Figure 4) is indicated by the arrow. The hole spectrum in B was obtained as described in Figure 2.

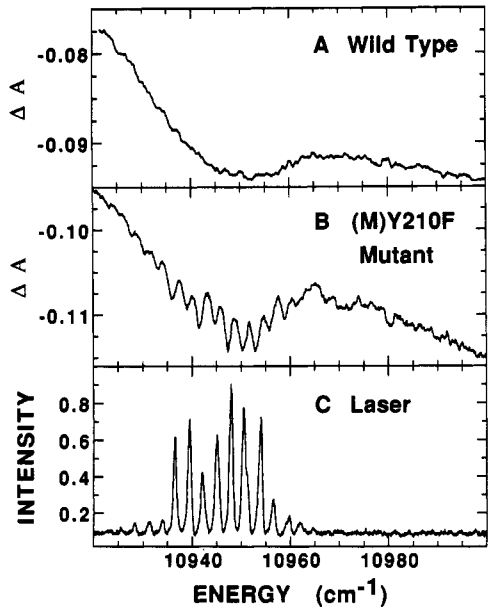

Figure 4. High-resolution view of the photochemical hole-burning spectra of (M)Y210F and wild-type *Rb. sphaeroides* RCs in the vicinity of the group of lines generated by the laser diode. The output spectrum of the laser diode used to burn the holes is shown in the bottom panel. The monochromator resolution for these scans was 0.65 cm^{-1}. Laser power = 5 mW/cm^2.

emission provide an internal calibration for the resolution of the system. A well-resolved set of zero-phonon holes (barely visible in Figure 3) is seen in the high-resolution ΔA spectrum of (M)Y210F RCs, with each hole corresponding to a line in the emission spectrum of the laser diode. In contrast to this result, individual zero-phonon features are not resolved in the hole spectrum of WT RCs (cf. Figure 2); rather, a broadened line shape corresponding to the sum of overlapping zero-phonon holes burned by each of the laser lines is observed. Thus at a qualitative level the zero-phonon hole widths in (M)Y210F RCs must be significantly less than the spacing between the laser diode lines (~3 cm^{-1}), while in the wild type the widths of these features must

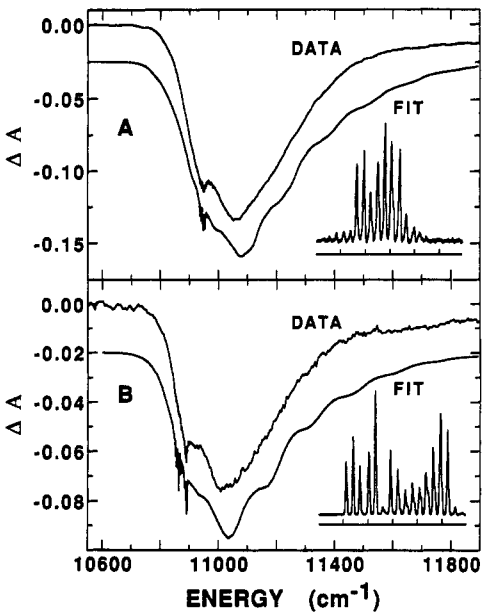

Figure 5. Wavelength dependence of photochemical hole-burning spectra in (M)Y210F. In each panel, the upper spectrum is an experimental hole-burning spectrum and the lower spectrum is a simulated spectrum, displaced vertically for clarity. The experimental spectra in A and B were obtained by using different laser diode burn sources; the laser output is shown in the lower right corner of each panel (total scale of each inset is 60 cm^{-1}).

be comparable to or broader than the laser line spacing.

The zero-phonon holes shown in Figure 4 are broadened due to two effects. First, adjacent zero-phonon holes partially overlap. This is certainly true in WT RCs, where no substructure due to the multiple burn laser lines is observed in the high-resolution hole scans. In (M)Y210F, partial overlap of neighboring holes is evidenced by the fact that the zero-phonon holes are not resolved down to the background slope of the broad hole. Second, each zero-phonon hole is broadened due to the finite bandwidth of the burn and probe beams. In order to extract the true zero-phonon hole widths, these two broadening effects must be accounted for quantitatively and deconvolved from the data. The overlap between zero-phonon holes was eliminated by fitting the high-resolution hole spectrum in the vicinity of the laser lines to a sum of Lorentzians[42] with center positions determined by the burn frequencies. A linear baseline was used in the fit to remove the background due to the broad hole, which has a nearly constant slope over the ~25-cm^{-1} span of the burn lines. In (M)Y210F the line widths of the Lorentzians determined from the least-squares fit to the 10 zero-phonon holes with the best signal to noise were (average ± SD) (2.0 ± 0.2)-cm^{-1} fwhm. The intrinsic zero-phonon hole widths were then determined by deconvolving the monochromator and burn laser line width functions from these component Lorentzians. At such high resolution (0.65 cm^{-1}), the monochromator throughput is best modeled by a Gaussian function.[43] The lines in the laser emission spectrum[44] were fit best by Lorentzian functions with a fwhm of 0.5 cm^{-1}. The Gaussian and Lorentzian contributions to the hole width were deconvolved by using the method described in ref 45. Assuming that the true zero-phonon hole shape is Lorentzian, an intrinsic hole width of (1.25 ± 0.25)-cm^{-1} fwhm is deduced for (M)Y210F RCs. This line width corresponds to an excited-state lifetime of

(42) Technically, the observed zero-phonon hole shapes should be Voight profiles (the function obtained from convolving a Gaussian with a Lorentzian). However, the Lorentzian component to the hole dominates, so the use of Lorentzian line shapes is a close approximation to the true line shape.

(43) Sundius, T. *J. Raman Spectrosc.* **1973**, *1*, 471.

(44) The laser line widths were determined by measuring emission spectra of the diodes with 0.3-cm^{-1} monochromator resolution. The laser line widths of 0.5-cm^{-1} fwhm are the values after deconvolution of the monochromator bandwidth (assumed Gaussian).

(45) Davies, J. T.; Vaughan, J. M. *Astrophys. J.* **1963**, *137*, 1302.

8.5 ± 2.0 ps.[46] The same analysis applied to the high-resolution hole-burning data on WT RCs yielded an intrinsic hole width of (8.7 ± 2.0)-cm^{-1} fwhm, corresponding to an excited-state lifetime of 1.2 ± 0.3 ps.

An additional advantage of using a burn laser with multiple emission lines is that the hole spectrum as a function of frequency can be measured with great accuracy. The envelope of the emission lines for these diodes is typically ~25 cm^{-1}, or ~2 nm, in width. We have also obtained hole-burning spectra for the (M)Y210F mutant using several different laser diodes, extending the range of experimental burn wavelengths from 10960 to 10850 cm^{-1}. As shown in Figure 5, as the burn wavelength is moved to lower energy, the zero-phonon hole amplitude decreases more rapidly than can be accounted for from the sample absorption and laser intensities. This anomaly is further discussed below. The zero-phonon hole widths, on the other hand, are independent of wavelength to within the signal to noise.

Discussion

Theoretical Model. There are a number of features in the absorption and hole-burning data that must be accounted for simultaneously in a satisfactory model for the absorption band of P. These include the width and asymmetry of the special pair absorption band at 1.5 K, the width and relative intensities of the narrow and broad components of the hole spectrum, the lack of resolved structure in the broad component of the hole, and the wavelength dependence of the broad[9,10] and narrow hole intensities. The analysis of the zero-phonon hole widths was described above. We have quantitatively analyzed the overall 1.5 K absorption and hole-burning line shapes by using a linear electron–phonon coupling model.[47,48] This is the same method used by Hayes and Small,[16,17,37,38] with some modifications, and a notation similar to that in refs 16 and 17 is used to facilitate comparison. This treatment assumes that only a single electronic state contributes to the P absorption band and is briefly outlined in the following paragraphs. An alternative theoretical treatment of the P absorption and hole band shapes, which explicitly includes other electronic states in the RC, has been presented by Won and Friesner.[39]

The single-site absorption spectrum is the spectrum that would be observed if all of the molecules in the sample were in identical environments. Its shape is determined by the widths and intensities of the vibrational and phonon transitions that couple to the P → ^{1}P electronic transition. For a transition in which only one harmonic mode is coupled, the single-site absorption spectrum $G(\Omega - \nu)$ is given in the $T = 0$ limit[49] by

$$G(\Omega - \nu) = \sum_{r=0}^{\infty} \frac{S^r e^{-S}}{r!} g_r(\Omega - \nu - r\omega) \qquad (1)$$

where Ω is frequency, $g_r(\Omega - \nu - r\omega)$ is a normalized line-shape function for the $0 \rightarrow r$ vibronic transition, and ω is the frequency of the coupled mode. The single-site spectrum as described by eq 1 consists of a sum of such vibronic transitions, each weighted by a Franck–Condon factor. The Franck–Condon factor for each vibronic transition depends on r and on the Huang–Rhys factor[47] S, which is a measure of the strength of the electron–phonon coupling. The weighting factors for the $g_r(\Omega - \nu - r\omega)$ are Poisson-distributed, with a maximum at approximately $r = S$. For example, for a mode with an S of 4, the $0 \rightarrow 4$ vibronic transition will be the most intense one in the progression. The weighting factor for the zero-phonon transition ($r = 0$) is simply e^{-S}.

The absorption spectrum is obtained by convolving the single-site spectrum with an inhomogeneous line-shape function $N_0(\Omega - \nu_m)$:

$$A(\Omega) = \int_0^{\infty} d\nu\, N_0(\nu - \nu_m) G(\Omega - \nu) \qquad (2)$$

The inhomogeneous distribution describes the variation in 0–0 transition energies of the chromophores due to slight differences in their interactions with their environments; it is characterized by a width and by a center frequency ν_m, which is the most probable 0–0 transition energy.

In order to evaluate eq 2, specific functional forms must be chosen for $N_0(\Omega - \nu_m)$ and for the $g_r(\Omega - \nu - r\omega)$. Zero-phonon lines are generally Lorentzian in shape.[50] Relatively little information exists on the shape of the higher vibronic transitions for large molecules in condensed phases. The inhomogeneous line shape for such systems is generally Gaussian, reflecting a statistical distribution of site energies. Analytical solutions for the integral in eq 2 exist if the functions are both Gaussians or both Lorentzians but not if a combination of the two is used.[45,51]

We have found (vide infra) that the long-wavelength side of the absorption spectrum of P cannot be fit well unless $N_0(\Omega - \nu_m)$ is Gaussian. Thus, we choose

$$g_r(\Omega - \nu - r\omega) = \frac{1}{(2\pi)^{1/2}\sigma_r} \exp\left\{\frac{-(\Omega - \nu - r\omega)^2}{2\sigma_r^2}\right\} \qquad (3)$$

and

$$N_0(\Omega - \nu_m) = \frac{1}{(2\pi)^{1/2}\sigma_I} \exp\left\{\frac{-(\Omega - \nu_m)^2}{2\sigma_I^2}\right\} \qquad (4)$$

which are normalized Gaussians with standard deviations of σ_r and σ_I, respectively. For this choice of shape functions, the integration indicated in eq 2 is straightforward and yields

$$A(\Omega) = \frac{1}{(2\pi)^{1/2}} \sum_{r=0}^{\infty} \frac{S^r e^{-S}}{r!} \frac{1}{\sigma_A} \exp\left\{\frac{-(\Omega - \nu_m - r\omega)^2}{2\sigma_A^2}\right\} \qquad (5)$$

where $\sigma_A^2 = (\sigma_r^2 + \sigma_I^2)$. Several limitations are built into this theory. First, because the r-phonon transition for each mode is calculated by an r-fold convolution of the 1-phonon transition, the line widths σ_r of the higher phonon transitions increase monotonically by the factor $r^{1/2}\sigma_1$.[48] There is little experimental evidence on the dependence of the vibrational width on quantum number for condensed-phase systems. Vibronic hole-burning studies on porphyrins, which are chemically similar to the bacteriochlorophyll chromophores in the special pair, indicate that the vibrational line widths do not increase in a regular or even monotonic fashion.[52] It should also be noted that the molecular parameters are assumed to be constant across the band. There is evidence that parameters such as S may vary significantly for different chromophores embedded in noncrystalline solids, reflecting the inherent disorder in glassy hosts.[51]

The hole spectrum is obtained by calculating the difference between the absorption spectrum before burning (eq 2) and after burning. The effect of burning for a time τ at frequency ω_B with a laser intensity I is to reduce the relative number of absorbers at any frequency ν from $N_0(\nu - \nu_m)$ to $N_\tau(\nu - \nu_m)$. The latter is given in the short burn time limit[53] by

$$N_\tau(\nu - \nu_m) = N_0(\nu - \nu_m)\{1 - \sigma I \Phi \tau [G(\omega_B - \nu)]\} \qquad (6)$$

(46) The hole width H is related to the homogeneous linewidth $\Delta\nu_{homo}$ and the excited-state lifetime T_1 by the relation $^1/_2H = \Delta\nu_{homo} = 1/\pi cT_2 = 1/2\pi cT_1 + 1/\pi cT_2^*$, where H and $\Delta\nu_{homo}$ are fwhm values in cm^{-1}, T_2 and T_2^* are the total and pure dephasing times, respectively, and c is the speed of light. If the pure dephasing contribution to the width is negligible (it is generally much less than 1 cm^{-1} in large molecules at 1.5 K), then the zero-phonon hole width can be related directly to the excited state lifetime T_1. Spectral diffusion on the timescale of the measurement may also add to the width of the hole, but this contribution to the hole width is also generally much less than 1 cm^{-1} at 1.5 K.

(47) Huang, K.; Rhys, A. *Proc. R. Soc. London* **1951**, *A208*, 352.

(48) Pryce, M. H. L. In *Phonons in Perfect Lattices and in Lattices with Point Defects*; Stevenson, R. W. H., Ed.; Oliver and Boyd: London, 1965; pp 403–448.

(49) The $T = 0$ approximation is valid if the lowest frequency mode that is coupled to the transition is much larger than kT (~1 cm^{-1} at 1.5 K).

(50) Burland, D. M.; Zewail, A. H. In *Advances in Chemical Physics*; Prigogine, I., Rice, S. A., Eds.; Wiley: New York, 1979; Vol. 40, p 369.

(51) Friedrich, J.; Swalen, J. D.; Haarer, D. *J. Chem. Phys.* **1980**, *73*, 705.

(52) Völker, S.; MacFarlane, R. M. *Chem. Phys. Lett.* **1979**, *61*, 421.

(53) The short burn time approximation is equivalent to assuming that the bleach is linearly proportional to the sample absorption at the burn wavelength and to the laser intensity. For the sample concentrations and burn powers used here, and the relatively narrow range of burn wavelengths from any of the laser diodes, the error introduced by making this approximation is less than 10%.

where σ and Φ are the absorption cross section and photochemical quantum yield, respectively, and $G(\omega_B - \nu)$ is the single-site spectrum evaluated at the burn frequency. The absorption spectrum after burning is then given by eq 2, with $N_r(\nu - \nu_m)$ substituted for $N_0(\nu - \nu_m)$. The hole spectrum is the difference between the burned and unburned absorption spectra:

$$\Delta A(\Omega) = -\sigma I \Phi \tau \int_0^\infty d\nu\, N_0(\nu - \nu_m) G(\omega_B - \nu) G(\Omega - \nu) \quad (7)$$

which upon integration yields

$$\Delta A(\Omega) = \frac{-\sigma I \Phi \tau}{2\pi\sigma_{HB}} \sum_{r=0}^{\infty} \sum_{r'=0}^{\infty} \frac{S^r e^{-S}}{r!} \frac{S^{r'} e^{-S}}{r'!} \exp\{[-(\Omega - \nu_m - r\omega)^2\sigma_r^2 - (\omega_B - \nu_m - r'\omega)^2\sigma_r^2 - (\Omega - \omega_B + \omega(r' - r))^2\sigma_I^2]/2\sigma_{HB}^2\} \quad (8)$$

where $\sigma_{HB}^2 = (\sigma_r^2\sigma_r^2 + \sigma_r^2\sigma_I^2 + \sigma_r^2\sigma_I^2)$. Within the linear electron–phonon coupling model, the absorption and hole line shapes are described completely by the vibronic and line-width parameters in eqs 5 and 8. These parameters, which include the width and center frequency of the inhomogeneous distribution function, the zero-phonon line width σ_0, and the Huang–Rhys factor S_i, frequency ω_i, and one-phonon width for all of the coupled modes i,[54] can *in principle* be deduced from self-consistent simulations of the absorption and hole line shapes. In the following, the results of such simulations are discussed. It is found that there are significant limitations to the precision with which some of these parameters can be determined from the simulations.

Simulations of Absorption Spectra. The 1.5 K absorption spectrum of (M)Y210F RCs was simulated by using eq 5 and a nonlinear least-squares fitting routine. As a starting point, we used the parameters deduced by Small and co-workers[16,17,55] from simulations of the P absorption and hole spectra for *Rb. sphaeroides* R-26 RCs. As in ref 17, it was found that the simulated spectrum accounts well for the low-energy half of the P band shape but falls off too rapidly immediately to the high-energy side of the peak. Variation of the parameters within the two-mode model failed to improve the quality of the fit significantly.

A likely source of the discrepancy *with significant consequences* for the hole-burning simulations is the inclusion of only two coupled modes in the calculation. Resonance Raman spectra[56] in the $\Delta\nu$ = 80–250-cm^{-1} region with excitation directly into the special pair absorption band at 12 K show two weak features at 102 and 138 cm^{-1}. More recent room temperature resonance Raman spectra[57] show lines with significant intensity at 95, 135, 200, 685, and 730 cm^{-1} and a possible feature at about 30 cm^{-1}. The absolute intensities for these bands, which would directly yield their Huang–Rhys factors, have not yet been reported. It should be noted that the frequencies of the resonance Raman bands are for the ground electronic state, whereas the excited-state frequencies are relevant to a complete analysis of the absorption and hole spectra. In order to account for the absorption on the high-energy side of the peak, a third mode with a frequency in the several hundred cm^{-1} range was included in the calculations. Although we could use the Raman frequencies for ω_i,[57] we prefer at this time to simply specify frequency ranges of the coupled vibrations that are consistent with the Raman data. Inclusion of a large number of modes in the calculation greatly increased the computation time and was not justified given the lack of resolved structure in the sideband component of the hole (vide infra).

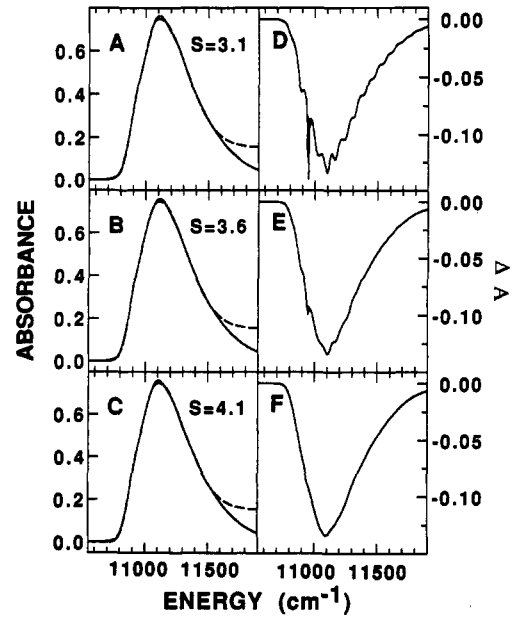

Figure 6. Panels A–C indicate the lack of sensitivity of the simulated 1.5 K absorption spectrum of (M)Y210F RCs to the magnitude of the vibronic coupling parameter S. The experimental spectrum is shown in each panel (---), along with simulated spectra (—), obtained by using eq 5 and three coupled modes for Huang–Rhys factors of (A) 3.1, (B) 3.6, and (C) 4.1. Other parameters were varied to yield the best fit to the data. Panels D–F indicate the high sensitivity of simulated 1.5 K photochemical hole-burning spectra for (M)Y210F RCs to the magnitude of S. Panels D, E, and F were calculated by using eq 8 and identical molecular parameters with panels A, B, and C, respectively.

Inclusion of the third mode greatly increased the quality of the absorption fits. An important parameter that we deduced from the simulations is the total electron–phonon coupling strength S_{total}. Representative simulations as a function of S_{total} are shown in Figure 6. In panels A–C of Figure 6, the experimental 1.5 K absorption spectrum of (M)Y210F RCs is indicated by the dashed lines, and simulated spectra are indicated by solid lines for total S values of 3.1, 3.6, and 4.1, respectively. In these simulations, the other parameters were allowed to vary freely to give the best fit to the absorption spectrum for each value of S_{total}. In other simulations (not shown) the quality of the fit was similar to those in Figure 6 for values of S_{total} ranging from less than 2 to greater than 5, which physically corresponds to a very large change in the electron–phonon coupling strength. The absorption line shape contains contributions from the homogeneous (single site) and inhomogeneous line shapes, and these two contributions can be played off against each other by varying the inhomogeneous width and the S_i and ω_i. Even for a constant value of the inhomogeneous line width and S_{total}, the individual S_i and ω_i could be varied significantly without degrading the quality of the absorption fit. Finally, changing the dependence of the higher vibronic widths on quantum number affects the asymmetry in the sideband component of the homogeneous spectrum for fixed values of the other parameters. In summary, fitting the low-temperature absorption spectrum alone was found to be an insensitive method for deducing the magnitude of the overall or the individual Huang–Rhys factors, the frequencies of the coupled modes, or the relative magnitudes of homogeneous and inhomogeneous broadening.

Simulations of Hole-Burning Spectra. Hole-burning spectra were calculated by using eq 8, modified to include three coupled modes.[54] The hole spectrum was calculated for each burn wavelength by using the experimental burn frequencies and intensities from the laser spectrum in Figure 4 and the wide range of vibronic and line-width parameter sets that are consistent with the 1.5 K absorption spectrum discussed in the previous section. The calculations were performed with a resolution of one point per 0.05 cm^{-1} in the region of the burn wavelength and one point

(54) In the separable harmonic limit (see: Myers, A. B.; et al. In *Biological Applications of Raman Spectroscopy*; Spiro, T. G., Ed.; Wiley: New York, 1987; Vol. 2, Resonance Raman Spectra of Polyenes and Aromatics, p 1), the Franck–Condon factors (FCFs) for a multimode system are given by the product of the appropriate single-mode FCFs, and the total electron–phonon strength is the sum of the single-mode Huang–Rhys factors. Thus the theory outlined for a single coupled mode is readily generalized to the case of an arbitrary number of coupled modes. The extension from one to two modes is shown explicitly in ref 16.

(55) These simulations included a low-frequency (~30 cm^{-1}) phonon mode and a low-frequency (115 cm^{-1}) "marker mode" of the special pair.

(56) Donohoe, R. J.; Dyer, R. B.; Swanson, B. I.; Violette, C. A.; Frank, H. A.; Bocian, D. F. *J. Am. Chem. Soc.* **1990**, *112*, 6716.

(57) Shreve, A.; Cherepy, N.; Franzen, S.; Boxer, S. G.; Mathies, R. A. *Proc. Natl. Acad. Sci. U.S.A.*, in press.

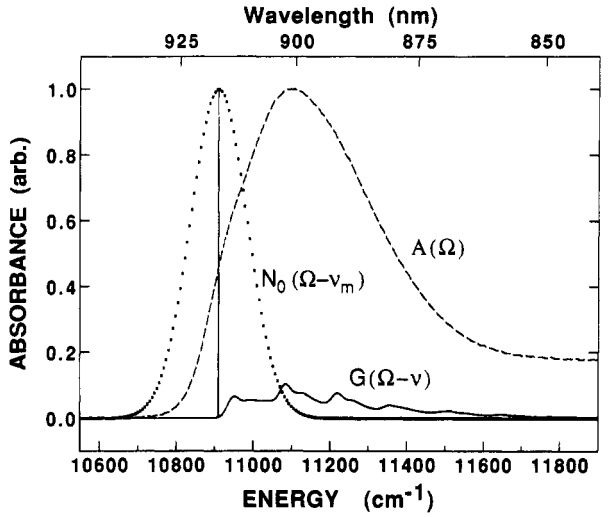

Figure 7. Relative contributions of homogeneous and inhomogeneous broadening to the P absorption band in (M)Y210F RCs at 1.5 K. A single-site absorption spectrum, $G(\Omega - \nu)$ (—), and Gaussian inhomogenous distribution function, $N_0(\Omega - \nu_m)$ (···), which are consistent with the hole and absorption spectra of (M)Y210F, are shown. The experimental absorption spectrum $A(\Omega)$ (---) is also shown. Very similar single-site spectra are obtained for other choices of the vibronic and line-width parameters; the range of acceptable parameters using a three-mode linear electron–phonon coupling model is given in Table I.

per 5 cm^{-1} away from the burn wavelength. The simulated hole spectra corresponding to each burn wavelength were then added together to produce the simulated hole spectrum corresponding to the multiline burn source. Model calculations are shown in Figure 6. The hole spectra in panels D–F of Figure 6 were calculated by using the same parameters as the corresponding absorption spectra in Figure 6A–C. The spectra indicate that the zero-phonon to phonon-sideband hole intensity ratio is extremely sensitive to the value of S_{total}. This ratio is $\sim\exp[-2S_{total}]$, depending on the burn wavelength, leading to the high sensitivity.[38] From these simulations, a value for S_{total} of 3.5 was deduced for (M)Y210F. Simulations of the hole and absorption spectra of WT RCs were best fit by using an S_{total} of 3.7. The value of S_{total} obtained from the simulations was not very dependent on the values of the other parameters or on the way in which S_{total} was divided among the S_i, as long as the parameters were also consistent with the absorption line-shape. The simulated hole profiles were very sensitive to the overall homogeneous broadening $\sum_i S_i\omega_i$. A reasonably precise value for the inhomogeneous line width σ_I could then be deduced, because σ_I and $\sum_i S_i\omega_i$ together determine the absorption width. The respective contributions of homogeneous and inhomogeneous broadening to the P band are illustrated in Figure 7, which shows the simulated single-site spectrum, $G(\Omega - \nu)$, and inhomogeneous distribution function, $N_0(\Omega - \nu_m)$, which are consistent with the experimental absorption and hole spectra of (M)Y210F. The experimental absorption spectrum $A(\Omega)$ for (M)Y210F RCs is also shown for comparison. The magnitudes of S_{total} and of the homogeneous and inhomogeneous broadening in the P band for WT and (M)Y210F RCs are given in Table I.

The simulations were less useful for determining precise values for the mode-specific parameters ω_i and S_i. This limitation is due to two factors. First, there is essentially no resolved vibronic structure in the hole or absorption spectra of the P band.[58]

TABLE I: Ranges of Vibronic and Line-Width Parameters for (M)Y210F and Wild-Type *Rb. sphaeroides* RCs at 1.5 K[a]

S_1	1.7–2.6
ω_1	20–50 cm^{-1}
S_2	0.5–1.2
ω_2	100–140 cm^{-1}
S_3	0.1–0.7
ω_3	150–500 cm^{-1}
Γ_I[b]	170–210 cm^{-1}
S_{total}	3.5–3.7

[a] Based on a three-mode linear electron–phonon coupling model with a single excited electronic state as described in the text. The frequency ω_i and coupling strength (Huang–Rhys factor) S_i for each coupled mode is indicated. [b] Fwhm of the inhomogeneous distribution function. For Gaussian line shapes, Γ_I is related to the standard deviation as $\Gamma_I = 2(2 \ln 2)^{1/2}\sigma_I$. The higher phonon line widths are all required to be >50 cm^{-1} to account for the lack of vibronic structure in the broad component of the holes.

Second, the number of modes that are coupled to the transition is not yet known, creating further difficulties in the determination of mode-specific parameters.[59] For the three-mode model used in our simulations, it was found that at least two moderately coupled (i.e., $S_i \geq 0.8$), low-frequency modes in the 30–200-cm^{-1} region as well as a third mode in the 150–500-cm^{-1} region with an S value in the range 0.1–0.7 were required to achieve a self-consistent fit of the absorption and hole-burning spectra. Ranges of the parameters that yield calculated absorption and hole spectra for (M)Y210F that are in agreement with the experimental spectra for (M)Y210F are listed in Table I. Simulations of the absorption and hole spectra for WT RCs (not shown) yielded parameter values within these same ranges. Our simulations do indicate that the basic physical model of strong coupling of low-frequency modes to the P → ^{1}P electronic transition[9,10,37-39] is consistent with the hole and absorption line shapes, and the ranges of mode frequencies in Table I are consistent with the available resonance Raman data.[56,57] As more modes are included in the simulations, the ranges of the individual mode parameters that are consistent with the data are expected to be even larger. Other measurements such as absolute resonance Raman intensities and excitation profiles are in progress to determine accurate values for the individual vibrational frequencies and coupling constants. These data, in combination with the hole-burning and absorption line shapes, can be used to develop a unified and detailed description of the mode structure and line broadening of an absorption band, as well as some aspects of the excited-state dynamics, as recently shown for rhodopsin and bacteriorhodopsin.[60]

It is possible to further test the strong coupled model by comparing the calculated and experimental spectra as a function of burn wavelength. Two counterbalancing effects determine the hole intensity at any burn wavelength. The first trivial effect is that the absorption of the sample is different at each wavelength and so the number of photons absorbed, and hence the hole depth, will be different (the slope of A is very steep at the low-energy edge of the spectrum). The other effect is that the magnitude of the zero-phonon hole relative to that of the broad sideband hole increases greatly as the excitation wavelength is moved to lower energy. Both of these effects are accounted for in eq 8. In Figure 5 the calculated and experimental hole spectra as a function of burn wavelength are compared for two hole-burning spectra obtained with different laser diode burn sources. As the burn wavelength approaches the extreme low-energy edge of the absorption band, the experimental zero-phonon holes decrease more

(58) We emphasize that even without precise values for the individual mode frequencies and coupling constants, the single-site spectrum is well-defined from the simulations. In the absence of resolved vibronic structure in the side-band component of the hole, there are a number of different combinations of frequencies, coupling constants, and vibronic line widths within the range specified in Table I that yield essentially identical single-site spectra. In addition, Figure 7 indicates that the slight amount of vibronic structure in the single-site spectrum is not preserved in the hole spectrum; i.e., the hole-burning experiment does not perform a perfect deconvolution of the homogeneous and inhomogeneous spectra.

(59) This latter uncertainty is actually a severe limitation, because in the separable harmonic approximation to the Huang-Rhys formalism a single mode of frequency ω and coupling constant S will give exactly the same single-site spectrum as two modes with frequencies of ω and coupling constants of $S/2$ (and in general, to n modes with frequencies of ω and coupling constants of S/n). Thus relatively weak coupling to a large number of modes with small S values has the same effect on the single-site spectrum as strong coupling to a smaller number of modes, if the frequencies of the modes in each case are similar.

(60) Loppnow, G. R.; Mathies, R. A.; Middendorf, T. R.; Gottfried, D. S.; Boxer, S. G. *J. Phys. Chem.*, submitted for publication.

rapidly in intensity than the simulated holes. A wavelength dependence to the overall Huang–Rhys factor or the quantum yield for formation of the long-lived species P^+Q^- may explain the discrepancy. These effects could be the result of more than one transition under the P band; however, the data do not provide definitive evidence for or against the presence of another electronic state. There is a shoulder on the low-energy side of the special pair absorption band, which is only apparent at liquid helium temperatures; this has been variously attributed to a separate electronic transition,[40,61,62] heterogeneity in the RC,[63,64] and vibronic structure within a single electronic transition.[16,17] Stark effect spectra obtained at 1.5 K are presented elsewhere and further address this unresolved question.[65,66]

A final point concerns the large vibronic line widths required to fit the hole spectra. In agreement with other workers,[16,17] we have found that rather broad one-phonon line widths (>30 cm^{-1} for the low-frequency mode and >50 cm^{-1} for the other modes) are required in the hole simulations in order to remove a vibronic satellite structure. It should be borne in mind that the vibrational manifold resulting from the inclusion of only two or three modes will be rather sparse, and therefore vibrational line widths that are comparable to the vibrational spacings are required to eliminate substructures in the hole. The requirement of broad vibrational line widths thus depends on the number of modes that is used in the calculation and on their relative frequencies and coupling constants. In the absence of such information, we simply note that if a large number of modes are actually coupled (particularly in the low-frequency region), the vibronic line widths obtained from these simulations may be overestimated. The most recent Raman data indicate at least five coupled modes.

Implications of Lifetime-Limited Zero-Phonon Hole Widths. For both (M)Y210F and WT RCs, the excited-state lifetime of ^1P deduced from the zero-phonon hole widths agrees quantitatively with the low-temperature lifetime measured directly in transient absorption experiments.[18,36] This agreement has important consequences for the electronic dynamics, and possibly for the vibrational dynamics, of the photoexcited special pair prior to electron transfer.

The hole-burning results provide direct information on the electronic dynamics of the special pair immediately following photoexcitation. The zero-phonon hole width is a state-selective measurement, because this width is solely determined by the total dephasing time of the lowest vibrational level of the electronic state ^1P. Two points should be stressed: the zero-phonon hole width is insensitive to the dynamics of the higher vibrational levels of ^1P, and it is determined by the most rapid relaxation channel of the zero-point level of ^1P.

The possibility of electronic decay of ^1P before the initial electron transfer reaction occurs has been considered by several groups.[9-12] A growing body of experimental evidence suggests that subpicosecond electronic relaxation of ^1P does not take place. First, transient absorption measurements indicated that the lifetime of the stimulated emission from ^1P decays with the same time constant as the bleach of the bacteriopheophytin ground-state absorption and rise of the H_L anion.[4,36] The agreement between the two observables was attributed to simultaneous formation of P^+ and H_L^-. If ^1P decays faster than $P^+H_L^-$ is formed, then the absorption and emission spectra would have different kinetics.[67] Second, previous measurements of the effect of an applied electric field on the fluorescence from *Rb. sphaeroides* RCs[68,69] led to the conclusion that ^1P does not decay into an electronic state with a larger dipole moment during its lifetime. The hole-burning measurement is less restrictive than either of these observables because the zero-phonon hole width is determined by the most rapid relaxation of ^1P. The results reported here indicate that in both (M)Y210F and WT RCs the most rapid decay of ^1P occurs with the same rate as the decay of the stimulated emission from ^1P. Electronic relaxation of ^1P with a rate that is faster than the rate of the process that competes with stimulated emission (assumed to be the initial electron transfer) is therefore ruled out. Because the zero-phonon hole width is sensitive only to the decay time of ^1P, not the identity of the state to which it decays, these results provide no information on the identity of the initial-electron acceptor.

The agreement between the zero-phonon hole width (which measures the decay time of the lowest vibrational level of ^1P) and transient absorption measurements (which indicate the overall decay time of the ^1P manifold) may also have implications for the vibrational dynamics of ^1P on the excited-state surface. For a molecule with strong electron–phonon coupling like P, only a tiny fraction of the sample is excited directly into the zero-phonon level of ^1P. Rather, most of the initially excited molecules contain a large amount of excess vibrational energy (~200–300 cm^{-1}), and immediately after photoexcitation the sample is characterized by a broad distribution of initial vibrational-state populations (see Figure 7). If the rate of the initial electron transfer reaction in RCs depends on the initial vibrational state of the reactant and on the free energy difference between reactants and products, then it is surprising that the rate of electron transfer from the zero-phonon level of ^1P is equal to the net rate from the vibrationally hot ^1P manifold.

Small et al.[16,17] have rationalized the agreement between the time and frequency domain experiments on WT RCs by proposing that the "marker mode"[55] thermalizes prior to the initial electron transfer but did not specify whether this refers to intramolecular vibrational relaxation (IVR), in which the excess vibrational energy initially in this mode is randomized among the various vibrational modes of P, or vibrational cooling, in which this energy is dissipated from P into the solvent. The relaxation time of the ~30-cm^{-1} phonon mode[55] was not discussed by these authors. We note that if vibrational cooling for *all* of the coupled modes is faster than the initial electron transfer rate, then ^1P will be in thermal equilibrium with the surrounding bath, which at 1.5 K corresponds to the lowest vibrational level of ^1P being populated to the exclusion of all other levels. The agreement between the hole burning and kinetics measurements follows immediately in such a scheme, since electron transfer always occurs from the zero-phonon level of ^1P, no matter how much excess vibrational energy was initially deposited during absorption.

In the following, we outline an alternative proposal, which is also consistent with the experimental data. As mentioned above, an important consideration is the dependence of the rate of the initial electron transfer reaction on the free energy difference for the reaction. Recent measurements of the effect of an applied electric field on the initial electron transfer rate[26] as well as studies of several RC mutants with considerably smaller driving force than WT indicate only a mild dependence of the rate on ΔG.[21,23,70] We conclude that it is not necessary to invoke ultrafast vibrational cooling prior to electron transfer in order to understand the agreement between the time and frequency domain measurements. Rather, the data are equally consistent with parallel and similar rates of electron transfer from a range of vibrational levels of ^1P.

Other experimental data may provide evidence related to the above hypotheses. The broad (>50-cm^{-1} fwhm) vibronic line widths that were required in the simulations of the hole spectra could be due to extremely short vibrational lifetimes in ^1P.[16,17] The <200-fs photon echo decays[11,12] observed for the P band could

(61) Vermeglio, A.; Paillotin, G. *Biochim. Biophys. Acta* **1982**, *681*, 32.
(62) Maslov, V. G.; Klevanik, A. V.; Ismailov, M. A.; Shuvalov, V. A. *Dokl. Akad. Nauk. SSSR* **1983**, *269*, 1217.
(63) Hoff, A.; Lous, E. J.; Moehl, K. W.; Dijkman, J. A. *Chem. Phys. Lett.* **1985**, *114*, 39.
(64) Parson, W. W.; Warshel, A. *J. Am. Chem. Soc.* **1987**, *109*, 6152.
(65) Mazzola, L. T.; Middendorf, T. R.; Boxer, S. G.; Gaul, D.; Schenck, C. C. *Biophys. J.* **1991**, *59*, 139a (abstract).
(66) Middendorf, T. R.; Mazzola, L. T.; Boxer, S. G.; Gaul, D.; Schenck, C. C., manuscript in preparation.
(67) The relaxation considered in this context is distinct from the question of whether the initial electron acceptor is B_L or H_L. In either case, the initial electron transfer from ^1P is believed to occur in ~1–3 ps.
(68) Lockhart, D. J.; Boxer, S. G. *Chem. Phys. Lett.* **1988**, *144*, 243.
(69) Lockhart, D. J.; Hammes, S. L.; Franzen, S.; Boxer, S. G. *J. Phys. Chem.* **1991**, *95*, 2217.
(70) Woodbury, N. W.; Taguchi, A. K.; Stocker, J. S.; Boxer, S. G. In *Reaction Centers of Photosynthetic Bacteria*; Michel-Beyerle, M.-E., Ed.; Springer-Verlag: Berlin, 1990; p 303.

also result from short vibrational T_1 times. In our view, the connection between the rate of vibrational cooling and the line width of vibronic transitions deduced from the simulations is rather tenuous, since these line widths (and the photon echo decay times) are determined by the total dephasing time of the excited-state vibrational level and thus contain contributions from pure dephasing processes as well as population decay. Even if the pure dephasing contribution could be neglected, the T_1 time may not be equal to the vibrational cooling time. Experimental measurements of vibrational cooling in metalloporphyrin monomers[71] and dimers,[72] which are reasonable models for the chromophores in the RC, and in dye molecules[73] indicate that this process requires several picoseconds, even at room temperature, while IVR generally occurs more rapidly.[74] Finally, as discussed earlier, the inclusion of only two or three modes for simplicity in the hole-burning simulations will likely result in overestimation of the vibronic line widths if in reality a larger number of modes are coupled. Since electronic relaxation of ^{1}P prior to electron transfer has been ruled out, the large Stokes shift measured for the P band suggests that some fraction of the excess vibrational energy in ^{1}P is dissipated into the solvent and thus that vibrational cooling has occurred to some extent prior to electron transfer (IVR alone would not lead to a Stokes shift). Further experiments such as measurements of the Stokes shift, fluorescence line shape, time-dependent shifts in the stimulated emission from ^{1}P, and absolute resonance Raman intensities of RCs under the same conditions as the experiments reported here are required to clarify the nature of the vibrational dynamics in ^{1}P.

Establishing the time scale for vibrational equilibration in ^{1}P may be of considerable importance in elucidating other aspects of the photochemistry in RCs, such as the weak temperature dependence of the initial electron transfer rate. In the limit that electron transfer occurs much faster than vibrational cooling in ^{1}P, the relative populations of initial vibrational levels of the reactant ^{1}P will be essentially independent of the bath temperature and thus so will the contribution of the nuclear (Franck–Condon) factors to the rate (these factors will depend on temperature only to the extent that the single-site line shape varies with temperature). This is a fundamentally different rationalization for the weak temperature dependence of the initial charge-separation reaction than is typically given. If electron transfer occurs much faster than vibrational thermalization, then a markedly non-Boltzmann distribution of vibrational populations must be included in theoretical calculations of the rate. This situation has been treated theoretically by Jortner,[75] and an interesting proposal concerning the rapid rate of the initial electron transfer reaction in the RC was also offered. In that work the calculated electron transfer rate is very rapid if photoexcitation of P populates vibrational levels of ^{1}P that are above the crossing point of the ^{1}P and $P^+H_L^-$ potential energy surfaces (the latter statement is equivalent to postulating moderate to strong electron–phonon coupling in the P absorption *if* the modes that are coupled to the P absorption are the relevant modes for the initial electron transfer). The calculated rate is greatly reduced for initial levels that are lower in energy than the energy at the crossing point of the two surfaces. In contrast to this prediction, our results indicate that electron transfer proceeds with a picosecond rate even from the lowest vibrational level of ^{1}P. Thus if the model in ref 75 is applicable at all, the crossing point of the surfaces must be near the bottom of the ^{1}P surface.

It is interesting that the Tyr(M)210 → Phe mutation slows the electron transfer rate by nearly an order of magnitude at low temperature yet has a negligible effect on the overall magnitude of the electron–phonon coupling. These observations may provide insights into the role of the charge transfer (CT) state $P^+B_L^-$ with respect to the electronic nature of ^{1}P, as well as the mechanism of the initial charge separation reaction. The magnitude of S_{total} in the special pair absorption band should be a particularly sensitive probe of the mixing with charge transfer configurations such as $P^+B_L^-$, because the strength of the linear electron–phonon coupling of a normal mode to an optical transition is proportional to the square of the displacement in equilibrium nuclear geometry between the ground and excited electronic states along the normal coordinate for the mode. Polarity changes between the electronic states connected by the transition are expected to give rise to such displacements, especially for those normal modes that involve motion in the direction that charge is displaced during photoexcitation. We assume that the primary effect of the Tyr(M)210 → Phe mutation is to raise the energy of $P^+B_L^-$ in (M)Y210F relative to the WT,[31] which implies that any changes in the CT character of ^{1}P that may result from the mutation can be attributed to changes in the mixing with $P^+B_L^-$. The similarity in the electron–phonon coupling strength for WT and (M)Y210F RCs (Table I) suggests that the coordinate displacements that occur upon photoexcitation are relatively unaffected by the mutation.

A more difficult question is the quantitative relationship between the degree of charge-transfer character in the excited state and the magnitude of the normal coordinate displacements. A first step in this direction was taken by Haarer in a study of electron–phonon coupling in organic charge-transfer crystals.[76] A simple electrostatic model was used to estimate the dependence of S on the charge displacement between the donor and acceptor molecules of the CT crystals. The one-mode model indicates that S varies as q^4/ω^3, where q is the fractional charge displaced upon excitation and ω is the frequency of the coupled mode. If we assume that the mode frequencies and the geometry of the dimer are the same in (M)Y210F and WT and that the coupled mode involves motion along the direction of charge separation (the largest possible effect), then the relative values of S_{total} for these two RCs can be used to estimate the relative degree of charge displacement upon excitation. From the results in Table I, S_{total} does not vary by more than about 10% between (M)Y210F and WT RCs. Thus, within this very simple model, the relative fraction of displaced charge varies by only a few percent between the two types of RC. A more exact analysis of the effect requires the identification of the modes that are coupled to the P → ^{1}P transition and a precise estimate of the energy of $P^+B_L^-$ relative to ^{1}P. Qualitatively, the similarity in S_{total} for (M)Y210F and WT suggests that the admixture of $P^+B_L^-$ in ^{1}P is not significantly affected by the Tyr → Phe mutation. The dipolar characteristics of ^{1}P in these RCs has also been investigated by Stark spectroscopy. The magnitude and line shape of the electroabsorption spectrum is quite similar for (M)Y210F and WT RCs, even at liquid He temperatures, where substantial substructure is observed in both.[65,66] Thus, we conclude that the CT state $P^+B_L^-$ is not a primary determinant of the electronic character of ^{1}P in either RC. It is likely then that the Tyr(M)210 → Phe substitution affects the initial electron transfer rate by decreasing the coupling between reactants and products or by altering the stability of the products of the reaction while exerting relatively little effect on the reactant ^{1}P.

Chan et al.[34] have recently measured the rate of the initial charge separation reaction in mutants of *Rhodobacter capsulatus* in which both Tyr(M)208 (analogous to Tyr(M)210 in *Rb. sphaeroides*) and Phe(L)181, the residue related by the local C_2 symmetry axis to Tyr(M)208, are changed. A slight enhancement of the rate was observed when Tyr replaced Phe(L)181 compared to wild-type *Rb. capsulatus* RCs. To explain this interesting result, these workers proposed that a tyrosine in position (L)181 stabilizes the special pair in some way (whether the effect is mostly on ^{1}P or P^+ was not specified) and imply more generally that changes in the symmetry-related (M)208/(L)181 residues largely affect the special pair. A direct comparison of this conclusion with our finding that changing Tyr(M)208 to Phe does *not* primarily affect ^{1}P is not possible because we have not yet studied the anomalous

(71) Rodriguez, J.; Holten, D. *J. Chem. Phys.* **1989**, *91*, 3525.
(72) Bilsel, O.; Rodriguez, J.; Holten, D. *J. Phys. Chem.* **1990**, *94*, 3508.
(73) Laermer, F.; Elsaesser, T.; Kaiser, W. *Chem. Phys. Lett.* **1989**, *156*, 381.
(74) Chang, T.-C.; Dlott, D. *J. Chem. Phys.* **1988**, *90*, 3590.
(75) Jortner, J. *J. Am. Chem. Soc.* **1980**, *102*, 6676.
(76) Haarer, D. *J. Chem. Phys.* **1977**, *67*, 4076.

mutant. It may well be that the Phe(L)181 → Tyr mutation in *Rb. capsulatus* primarily affects ^{1}P, but this does not appear to be the case for Tyr(M)210 → Phe in *Rb. sphaeroides*.

Acknowledgment. We thank Drs. Larry Takiff, Kathy Meehan, Aland Chin, and Tom Haw of Polaroid Corp. for their generous gift of the laser diodes used in these experiments. This work was supported by grants from the NIH FIRST and a Research Career Development Award (C.C.S.), the donors of the Petroleum Research Fund (C.C.S.), administered by the American Chemical Society, and the National Science Foundation Biophysics Program (S.G.B.).

Structural Study of Polyaniline Films in Reprotonation/Deprotonation Cycles

K. G. Neoh,* E. T. Kang,

Department of Chemical Engineering, National University of Singapore, Kent Ridge, Singapore 0511

and K. L. Tan

Department of Physics, National University of Singapore, Kent Ridge, Singapore 0511
(Received: May 10, 1991)

The structures of emeraldine base films, cast from *N*-methylpyrrolidinone solution, after being subjected to varying levels of reprotonation and repeated reprotonation/deprotonation are studied using X-ray photoelectron spectroscopy and infrared absorption spectroscopy. Two acids, HCl and $HClO_4$, have been tested, and the results indicate that with the latter the amine units of the film can be protonated much more readily than those of the powder sample. For highly protonated films, structural modifications resulting in a higher intrinsic oxidation state are apparent after one reprotonation/deprotonation cycle. The structural modifications have also resulted in the solubility of the films being drastically reduced. By the third reprotonation cycle, the interactions of the anions with the then structurally modified polymer films have resulted in chlorine species of distinctly different nature from those of the first two cycles. In contrast, the powder samples after three reprotonation/deprotonation cycles show no significant deviation from the pristine base.

Introduction

The structure of the polyaniline family can be denoted as $[(-BNHBNH-)_{1-Y}(-BN{=}Q{=}N-)_Y]_n$, where B represents a benzenoid ring while Q represents a quinoid ring. The oxidation state of the polymer can be varied from the fully reduced state ($Y = 0$) or leucoemeraldine (LM) to the fully oxidized state ($Y = 1$) or pernigraniline. The 50% oxidized polymer has been termed emeraldine (EM) base.[1] This family of polymers has attracted considerable interest because of its unique redox properties. The electrical conductivity of the polymer can be increased from about 10^{-11} S/cm to over 1 S/cm either by varying the number of electrons per repeat unit through oxidative doping or by the addition of protons associated with the nitrogen sites.[1-6] Another factor which may further enhance the use of polyaniline in potential electronic applications is its solution processibility. It has recently been reported that both EM base and its protonated form can dissolve completely in concentrated H_2SO_4.[7] The use of protonic acid dopants of large molecular size such as toluene-*p*-sulfonic acid in the chemical synthesis of polyaniline has also resulted in a salt soluble in common organic solvents.[8] The simultaneous polymerization and oxidation of aniline by copper(II) perchlorate also resulted in a conductive polymer which is soluble in DMSO.[9] Furthermore, EM base is partially soluble in THF, DMF, and DMSO and completely soluble in *N*-methylpyrrolidinone (NMP).[10]

The polyanilines and their complexes have been extensively studied by spectroscopic techniques such as X-ray photoelectron spectroscopy (XPS)[11-15] and infrared (IR) absorption spectroscopy.[16-19] Recent XPS studies[20-23] have demonstrated that the

(1) Chiang, J. C.; MacDiarmid, A. G. *Synth. Met.* **1986**, *13*, 193. MacDiarmid, A. G.; Chiang, J. C.; Richter, A. F.; Epstein, A. J. *Synth. Met.* **1987**, *18*, 285.
(2) MacDiarmid, A. G.; Chiang, J. C.; Halpern, M.; Huang, W. S.; Mu, S. L.; Somasiri, N. L. D.; Wu, W.; Yaniger, S. I. *Mol. Cryst. Liq. Cryst.* **1985**, *121*, 173.
(3) Diaz, A. F.; Logan, J. A. *J. Electroanal. Chem. Interfacial Electrochem.* **1980**, *111*, 111.
(4) Leclerc, M.; Guay, J.; Dao, L. H. *Macromolecules* **1989**, *22*, 649.
(5) Ray, A.; Asturias, G. E.; Kerschner, D. L.; Richter, A. F.; MacDiarmid, A. G.; Epstein, A. J. *Synth. Met.* **1989**, *29*, E141.
(6) Nakajima, T.; Harada, M.; Osawa, R.; Kawagoe, T.; Furukawa, Y.; Harada, I. *Macromolecules* **1989**, *22*, 2644.
(7) Andretta, A.; Cao, Y.; Chiang, J. C.; Heeger, A. J.; Smith, P. *Synth. Met.* **1988**, *26*, 383.
(8) Li, S.; Cao, Y.; Yue, Z. *Synth. Met* **1987**, *20*, 141.
(9) Inoue, M.; Navarro, E. R.; Inoue, M. B. *Synth. Met.* **1989**, *30*, 199.
(10) Angelopoulous, M.; Asturias, G. E.; Ermer, S. P.; Ray, A.; Scherr, E. M.; MacDiarmid, A. G.; Aktar, M.; Kiss, Z.; Epstein, A. J. *Mol. Cryst. Liq. Cryst.* **1988**, *60*, 151.
(11) Salaneck, W. R.; Lundstrom, I.; Hjertberg, T.; Duke, C. B.; Conwall, E.; Paton, A.; MacDiarmid, A. G.; Somasiri, N. L. D.; Huang, W. S.; Richter, A. F. *Synth. Met.* **1987**, *18*, 291.
(12) Snauwaert, R.; Lazzaroni, R.; Riga, J.; Verbist, J. J. *Synth. Met.* **1987**, *18*, 335.
(13) Munro, S. H.; Parker, D.; Eaves, J. G. *Springer Ser. Solid-State Sci.* **1987**, *76*, 257.
(14) Mirrezaei, S. R.; Munro, H. S.; Parker, D. *Synth. Met.* **1987**, *26*, 169.
(15) Hagiwara, T.; Demura, T.; Iwata, K. *Synth. Met.* **1987**, *18*, 317.
(16) Ohsada, T.; Ohnuki, Y.; Oyama, N.; Katagiri, G.; Kamisako, K. *J. Electroanal. Chem. Interfacial Electrochem.* **1985**, *161*, 399.
(17) Kim, Y. H.; Foster, C.; Chiang, J.; Heeger, A. J. *Synth. Met.* **1988**, *25*, 49.
(18) Cao, Y.; Li, S.; Xue, Z.; Guo, D. *Synth. Met.* **1986**, *16*, 305.
(19) Tang, J.; Jing, X.; Wang, B.; Wang, F. *Synth. Met.* **1988**, *24*, 231.
(20) Tan, K. L.; Tan, B. T. G.; Kang, E. T.; Neoh, K. G. *Phys. Rev. B* **1989**, *39*, 8070.
(21) Kang, E. T.; Neoh, K. G.; Khor, S. H.; Tan, K. L.; Tan, B. T. G. *J. Chem. Soc., Chem. Commun.* **1989**, 695.
(22) Kumar, S. M.; Gaillard, F.; Bouyssoux, G.; Sartre, A. *Synth. Met.* **1990**, *36*, 111.

0022-3654/91/2095-10151$02.50/0